MOLECULAR DYNAMICS MODELING OF NANOSECOND LASER ABLATION: TRANSCRITICAL REGIME

ALEXANDER A. SAMOKHIN[1], VLADIMIR I. MAZHUKIN[2,3], ALEXANDER V. SHAPRANOV[2,3], MIKHAIL M. DEMIN[2], ALEXEY E. ZUBKO[1]

[1]A.M. Prokhorov General Physics Institute, RAS, Moscow, Russia
e-mail: asam40@mail.ru, web page: http://www.gpi.ru/eng/

[2]Keldysh Institute of Applied Mathematics, RAS, Moscow, Russia
e-mail: vim@modhef.ru, web page: http://www.keldysh.ru/

[3]National Research Nuclear University "MEPhI", Moscow, Russia
web page: https://mephi.ru/eng/

Summary. Nanosecond laser ablation regime is investigated for the case of thin liquid Al film heated with constant radiation with intensities of G = 44, 66 and 110 MW/cm^2. The film dimensions are $x\times y\times z$ = 448.7×37.3×37.3 nm^3 with periodical boundary conditions in y-z directions. For G = 44 MW/cm^2, six consequent explosions can be discerned (including one on the film back side) and at later times $t \geq 4700$ ps, the film disintegrates into multiple fragments. For higher intensities the ablation regime resembles explosive boiling process only at small times (~ 400 ps) for G = 66 MW/cm^2 while at later times the ablation process is smooth even at subcritical temperature and pressure values. For G = 110 MW/cm^2, the ablation regime is smooth for all considered times (~ 1000 ps) while temperature and pressure in the film surpass its critical values (T_C = 7630 K, P_C = 1415 bar) approximately at t = 700 ps.

1 INTRODUCTION

Explosive boiling during nanosecond laser ablation was considered in several recent papers [1-5] as well as in many other papers during about the last half a century. Some additional references can be found e.g. in [6-9]. Despite the long investigation history the explosive boiling problem is not completely clarified yet because, in particular, usual continual approach [7] is not sufficient for detailed description of liquid-vapor phase transition in highly nonequilibrium conditions when irradiated matter is in strongly superheated state.

It should be noted also that homogeneous nucleation theory used for describing explosive boiling process in many papers (see e.g. [1-5,8] and ref. therein) is not applicable for the highly nonequilibrium conditions when the arising bubbles can not be considered as independent ones. Probably for this reason in the papers [1-5,8] devoted to explosive boiling no sufficient (if any) information is given about the pressure behavior in the process. More straightforward and adequate approach to the explosive boiling problem during laser ablation can be realized in the framework of molecular dynamic calculations.

Theoretical analysis of the nanosecond laser ablation was carried out with the help of molecular modeling [10-13] for thin metal films $x\times y\times z$ = 430×6.2×6.2 nm^3 with periodically boundary conditions in y-z directions. For different ablation regimes (surface evaporation,

2010 Mathematics Subject Classification: 82D15, 82D35, 82D80.
Key words and Phrases: Evaporation, Explosive boiling, Critical Point, Molecular Dynamics.

explosive boiling, spinodal decomposition, supercritical fluid expansion) were found for constant laser intensity G = 38.5-154 MW/cm^2.

In ref. [6] similar molecular dynamic calculations was performed for G = 33 MW/cm^2 for bigger sample $x\times y\times z$ = 448.7×37.3×37.3 nm^3. It was shown that the surface evaporation regime at early times than changes to explosive boiling process at the moments t = 1740, 2655, 4545 and 4995 ps. The results qualitatively confirm previous conclusion obtained for the sample with smaller y-z periodical dimensions [10] where for G = 38.5 MW/cm2 similar explosive boiling occur at t = 1040, 1440, 1640, 2000, 2340 ps. Bigger space-dimensions and irradiated time duration considered in the present paper permit to observe more space-time inhomogeneities of the ablation process compared with the smaller sample. In the present paper, nanosecond laser ablation regime is investigated for G = 44, 66 and 110 MW/cm^2.

2 STATEMENT OF THE PROBLEM

Laser radiation propagates from right to left and is normally incident on the free surface of the film. Computational domain dimensions are 1700×37.3×37.3 nm^3 with periodical boundary conditions in y-z directions. It contains part of the film with dimensions $x\times y\times z$ = 448.7×37.3×37.3 nm^3 (17.87 millions of atoms). Part of the radiation is absorbed by the electronic components, and as a result of inelastic collisions is transferred to the ion subsystem. By using periodic boundary conditions in the directions Y, Z the problem is effectively reduced to one-dimensional approximation along the X direction (for transport processes of laser radiation and energy into electronic subsystem).

Combined TTM-MD [14] model is used to describe the processes.

Energy balance of electron subsystem is described by continuum energy equation (1) supplemented by the equation of laser radiation transfer (2):

$$\frac{\partial \varepsilon_e}{\partial t} = -\left(\frac{\partial W_e}{\partial x} + g(T_e)(T_e - T_i) + \frac{\partial G}{\partial x} \right) \tag{1}$$

$$\frac{\partial G}{\partial x} + \alpha G = 0 \tag{2}$$

Here ε_e is the volume density of electron energy, T_e, T_i are the electron and ion temperatures, $g(T_e)$ is the electron-ion coupling coefficient, G is the intensity of laser radiation in the medium, $\alpha = \alpha(T_e, n_e)$ is the coefficient of absorption of laser radiation, $W_e = -\lambda_e \dfrac{\partial T_e}{\partial x}$ is the heat flux, $\lambda_e(T_e, T_i)$ is the electron heat conductivity coefficient.

The energy balance equation of the electron subsystem (1) was solved in the condensed medium using the finite-difference method. Zero heat flux $W_e = 0$ was used as a boundary condition at the surface of the film and its fragments.

The connection between electron energy and temperature was obtained using approximation via Fermi integrals [15].

3D molecular-dynamic modeling was used to describe the ion motion:

$$\begin{cases} \dfrac{d\vec{r}_j}{dt} = \vec{\upsilon}_j \\ m_j \dfrac{d\vec{\upsilon}_j}{dt} = \vec{F}_j^{emb} + \vec{F}_j^{heat} \end{cases} \qquad (3)$$
$$j = 1 \ldots N$$

Here $m_j, \vec{r}_j, \vec{\upsilon}_j$ are the mass, radius-vector and velocity of j-th ion respectively, $\vec{F}_j^{emb} = -\dfrac{\partial U(\vec{r}_1 \ldots \vec{r}_N)}{\partial \vec{r}_j}$ is the force acting at the j-th ion from other ions, $U(\vec{r}_1 \ldots \vec{r}_N)$ is the interaction potential for which embedded atom model (EAM) potential [16] was chosen. The energy transfer from the electron subsystem to the ion is given by:

$$\vec{F}_j^{heat} = \frac{m_j(\vec{\upsilon}_j - \langle\vec{\upsilon}\rangle)}{3k_B T_i n_i} g(T_e)(T_e - T_i), \qquad (4)$$

where $\langle\vec{\upsilon}\rangle$ is the mean ion velocity in the neighborhood of the j-th ion.

At the initial time $t = 0$ the film was assumed to be heated to the temperature of 6340K, electron and ion subsystems are in thermal equilibrium.

3 RESULTS AND DISCUSSION

Increasing of radiation intensity to G = 44 MW/cm^2 does not change significantly the initial stage of film heating and vaporization, compared with G = 33 MW/cm^2. The first explosive boiling occurs at t_1 = 945 ps with recoil pressure rise up to 600 bar as compared to about 400 bar due to surface evaporation at t = 750 ps as it as seen from fig. 1,2. This maximum pressure level persists for about 150 ps with increasing to 670 bar at t = 1095 ps.

After the first explosion t = 945 ps (fig. 2) no pronounced explosive boiling occurs up to the moment t = 1860 ps (fig. 4) when the pressure reaches value P_R = 740 bar. This pressure exceeds its previous values P_R = 540 bar at t = 1515 ps, P_R = 640 bar at t = 1605 ps and P_R = 600 bar at t = 1665 ps (fig. 3). Snapshot on fig. 3 also shows several droplets formed during and after the first explosion. The vertically elongated droplet forms is due to scale differences (by factor ~5) in x and z directions.

The second explosive boiling develops in a way somewhat similar to the fourth explosive boiling for the case of smaller sample which begins at t = 1760 ps [10] and gives rise to almost simultaneous formation of two fragments (or two bubbles). No counterparts of the second and the third explosive boilings which occur in the smaller sample [10] are visible in the considered here sample.

The third explosion (t = 2805 ps) results in pressure rise up to 870 bar in interval 2565-3030 ps while the pressure minimum between the second and the third explosion is 730 bar. The pressure minimum between the third and the fourth explosion boiling is 750 bar at t = 3375 ps. During and after the fourth explosive boiling ($t \geq$ 3720 ps) the pressure is about 900 bar.

The fifth explosive boiling at t = 4050 ps is accompanied by multiply density fluctuations which develop in the region much deeper (≈ 200 nm) in the sample than in the considered before explosive boiling (≈ 50 nm). Evolution of such multiply density fluctuations similar to spinodal decomposition is presented in fig.5-8. From fig.6 it is seen also explosive boiling process on the back side of the sample with pressure rise from 370 bar to 500 bar.

It should be noted that at t = 4740 ps the back side temperature (T = 6860 K) is lower than temperature values at irradiated surface at the moments of explosive boilings at t = 945 ps (T = 6870 K), t = 1860 ps (T = 7080 K), t = 2805 ps (T = 7120 K), t = 3720 ps (T = 7180 K), t = 4050 ps (T = 7190 K). The back side temperature at t = 4740 ps is also lower than the temperature in the middle of the film where however no explosive boilings occurs probably due to pressure effect.

For G = 66 MW/cm^2 initial ablation behavior is somewhat similar to explosive boiling process with some recoil pressure jump as at is seen from fig.9-11 while at later times (fig.12) the regime with subcritical pressure and temperature values becomes more smooth.

No explosive boiling is observed for G = 110 MW/cm^2 at subcritical temperature pressure values because corresponding density fluctuations have no time to develop. As expected critical and supercritical ablation regimes also demonstrate no prominent fluctuations.

4 CONCLUSIONS

Results obtained in the present paper demonstrate evolution of nanosecond ablation regime from explosive boiling to spinodal decomposition and supercritical fluid expansion for increasing laser intensity G = 44-110 MW/cm^2. At G = 44 MW/cm^2 five explosions occur at irradiated surface in the interval from 800 ps to 4400 ps where at later times multiply fragmentation develops which corresponds to spinodal decomposition. At the same time (t = 4740 ps) the six explosive boiling is observed at the film back side though the local temperature there have the lowest value in the film. Such a behavior is probably due to effect of pressure which has the lowest value in this region.

It should be noted that many papers [1-5,8] which deal with explosive boiling investigations present no sufficient information about recoil pressure behavior during the explosion. This situation may be partially due to differences in formulations of the problem and the method of its solution.

As it was already mentioned earlier some features of explosive boiling pressure behavior investigation can give important information on critical pressure values of irradiated targets [10,11,17].

The work was supported by the RSF (project 15-11-30039).

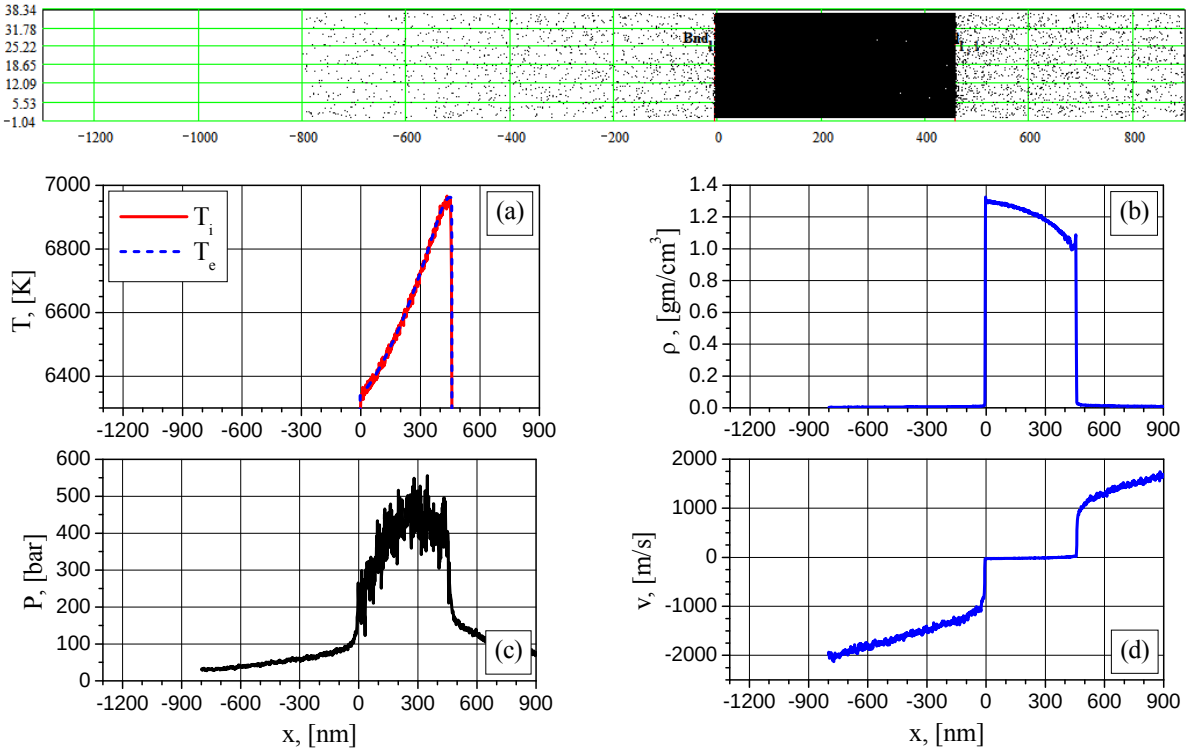

Fig. 1. 2D density particle distribution (snapshot) and 1D distributions of electron (blue) and ion (red) temperature (a), density (b), pressure (c), particle velocity (d) at the time of 750ps (G = 44 MW/cm^2).

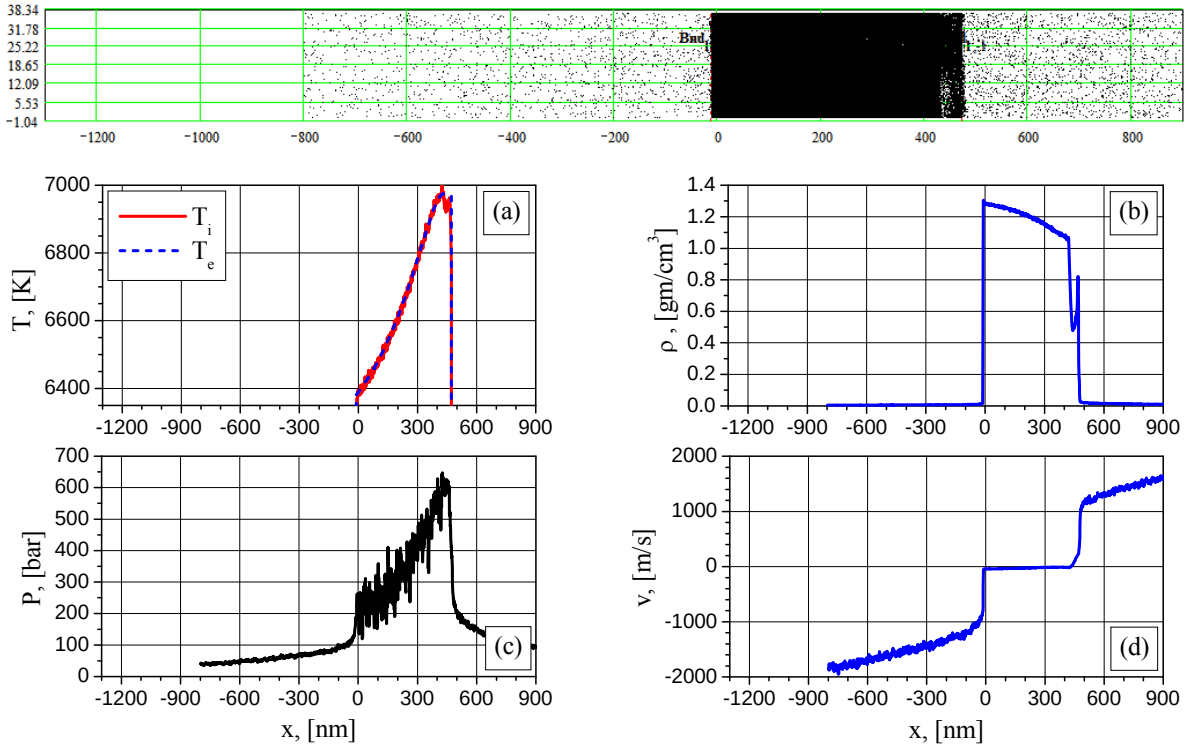

Fig. 2. 2D density particle distribution (snapshot) and 1D distributions of electron (blue) and ion (red) temperature (a), density (b), pressure (c), particle velocity (d) at the time of 945ps (G = 44 MW/cm^2).

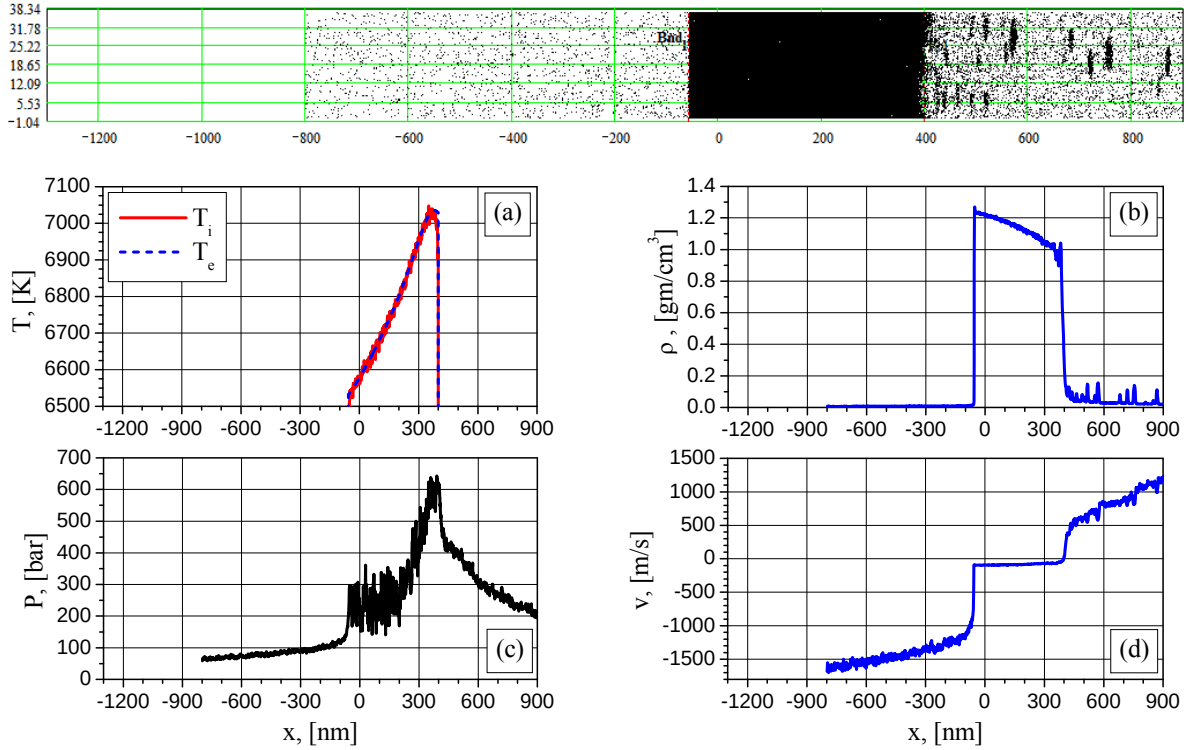

Fig. 3. 2D density particle distribution (snapshot) and 1D distributions of electron (blue) and ion (red) temperature (a), density (b), pressure (c), particle velocity (d) at the time of 1665ps (G = 44 MW/cm^2).

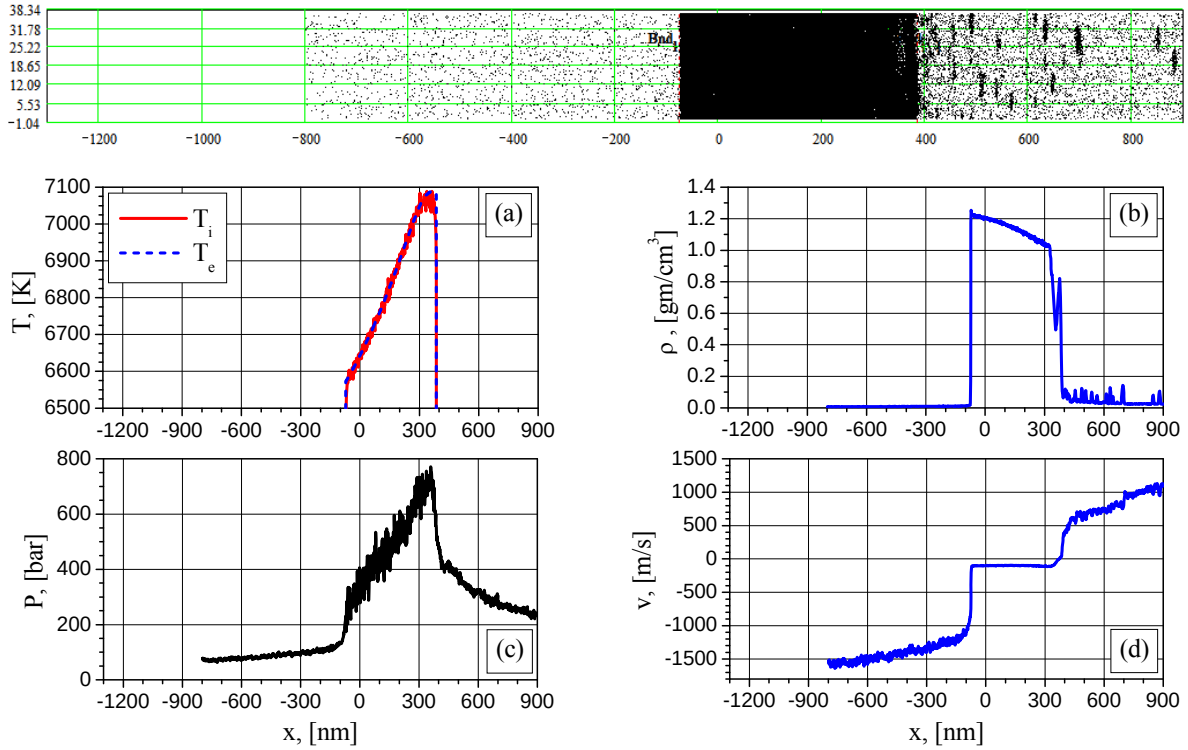

Fig. 4. 2D density particle distribution (snapshot) and 1D distributions of electron (blue) and ion (red) temperature (a), density (b), pressure (c), particle velocity (d) at the time of 1860ps (G = 44 MW/cm^2).

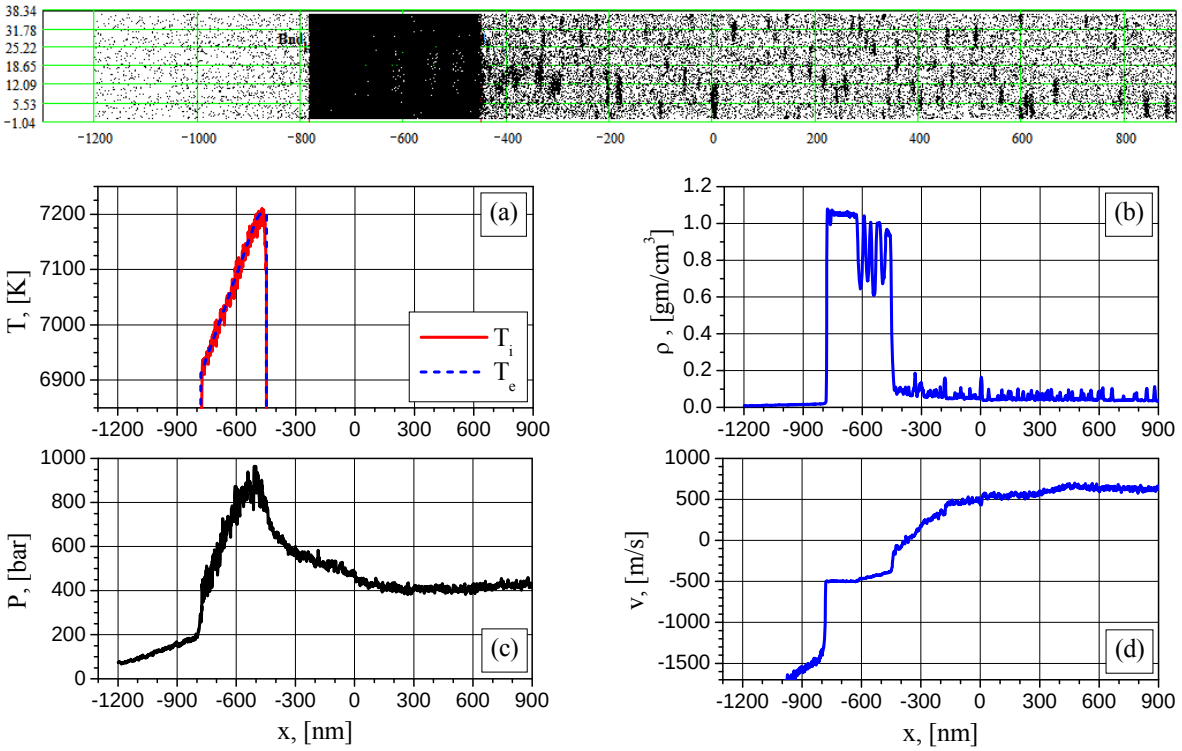

Fig. 5. 2D density particle distribution (snapshot) and 1D distributions of electron (blue) and ion (red) temperature (a), density (b), pressure (c), particle velocity (d) at the time of 4515ps (G = 44 MW/cm^2).

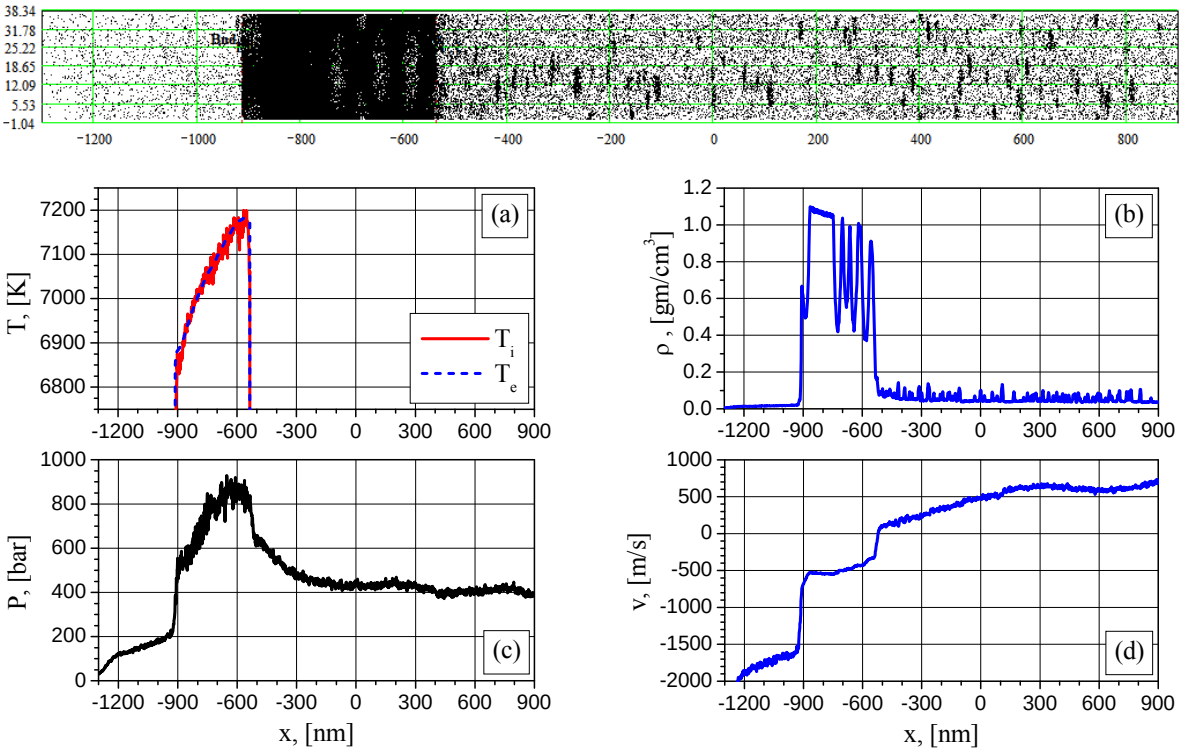

Fig. 6. 2D density particle distribution (snapshot) and 1D distributions of electron (blue) and ion (red) temperature (a), density (b), pressure (c), particle velocity (d) at the time of 4740ps (G = 44 MW/cm^2).

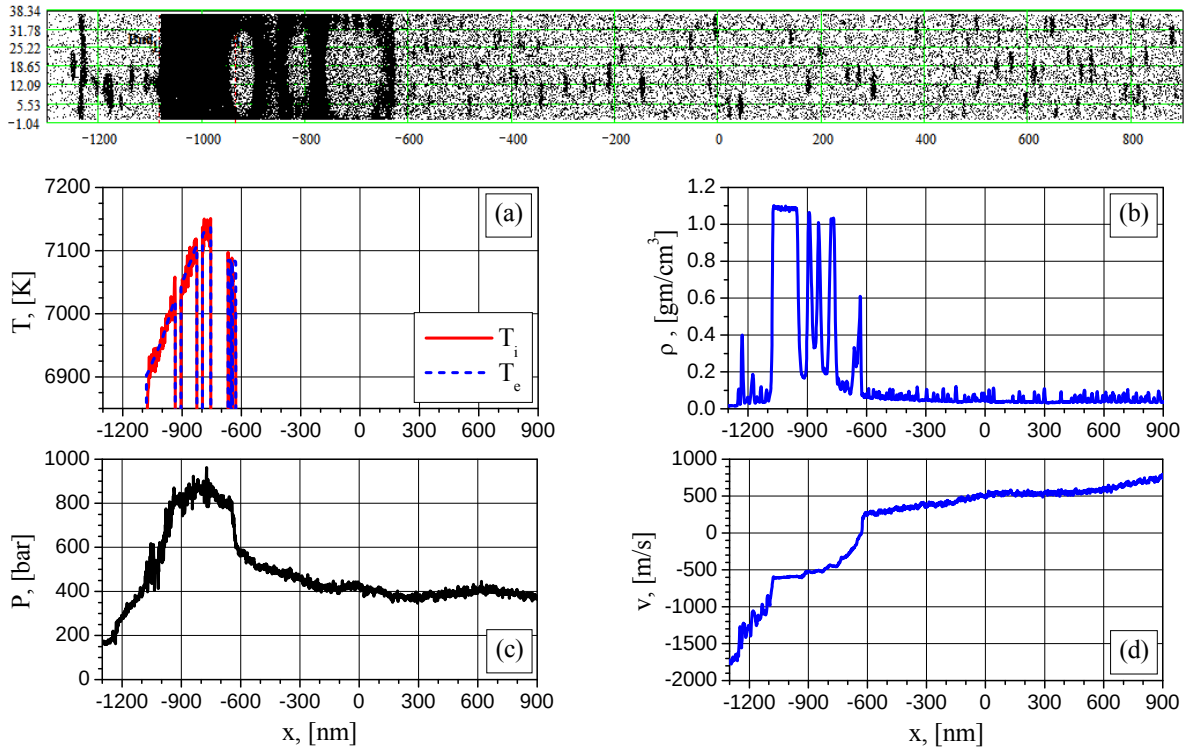

Fig. 7. 2D density particle distribution (snapshot) and 1D distributions of electron (blue) and ion (red) temperature (a), density (b), pressure (c), particle velocity (d) at the time of 5100ps (G = 44 MW/cm^2).

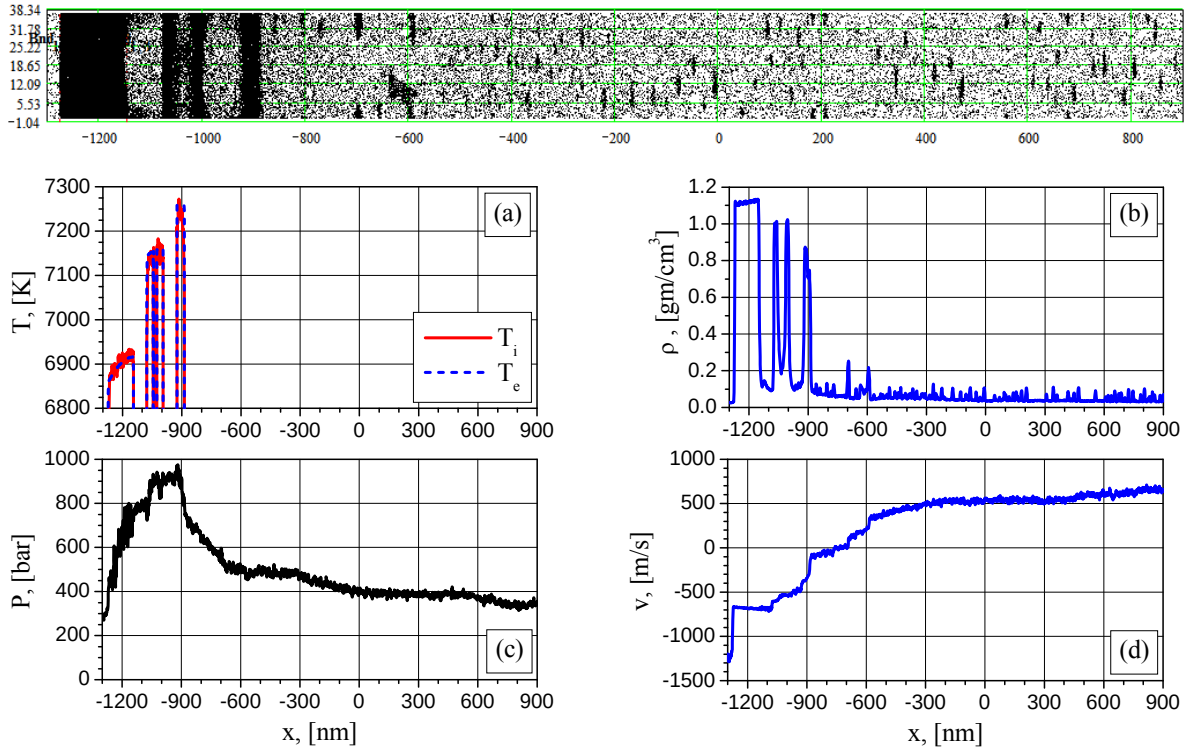

Fig. 8. 2D density particle distribution (snapshot) and 1D distributions of electron (blue) and ion (red) temperature (a), density (b), pressure (c), particle velocity (d) at the time of 5415ps (G = 44 MW/cm^2).

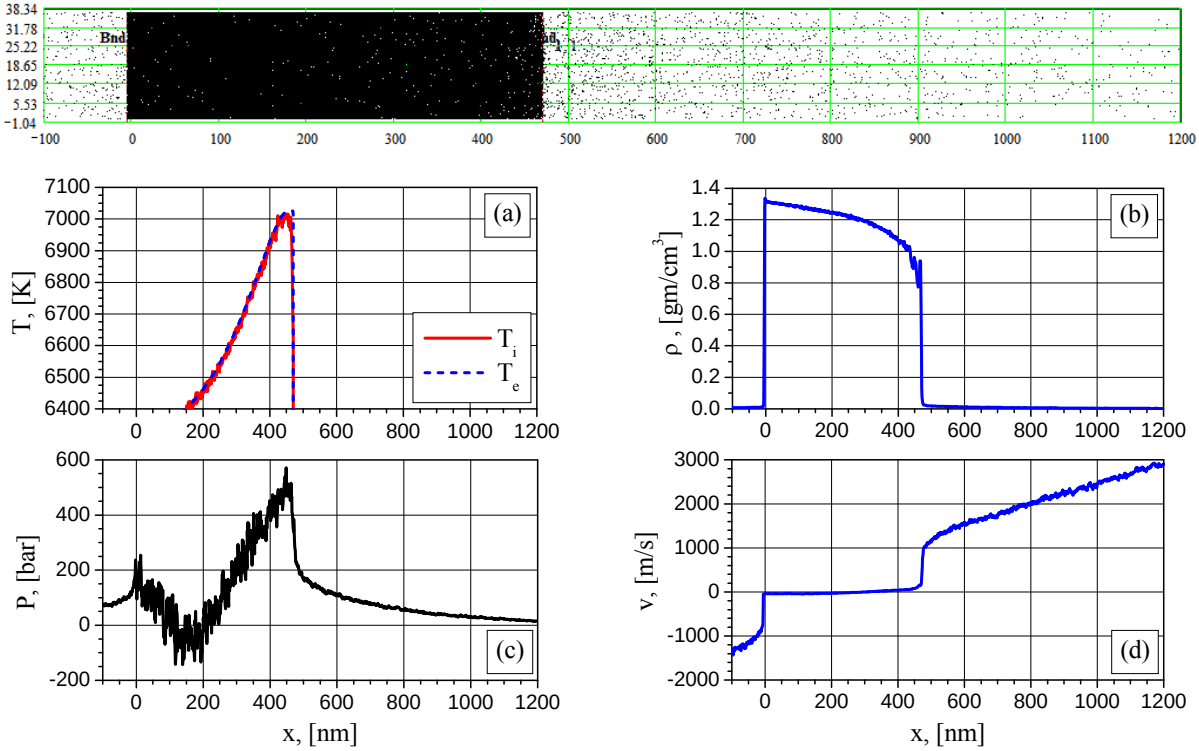

Fig. 9. 2D density particle distribution (snapshot) and 1D distributions of electron (blue) and ion (red) temperature (a), density (b), pressure (c), particle velocity (d) at the time of 375ps (G = 66 MW/cm^2).

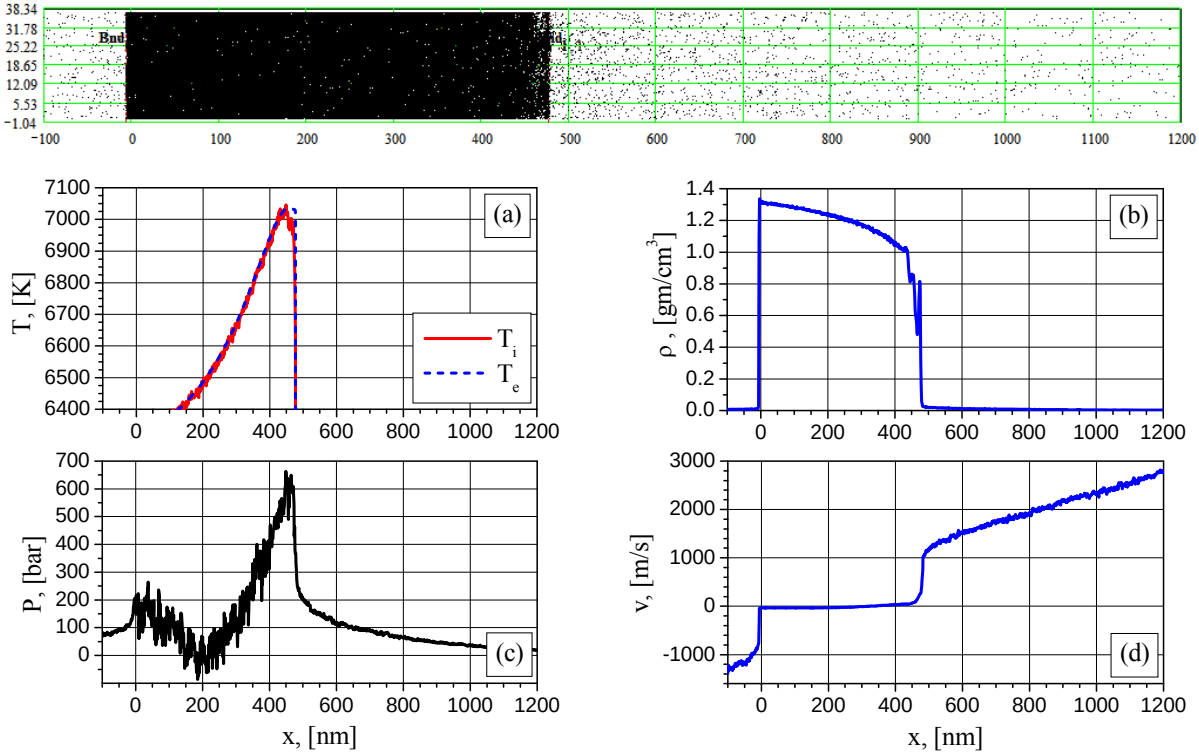

Fig. 10. 2D density particle distribution (snapshot) and 1D distributions of electron (blue) and ion (red) temperature (a), density (b), pressure (c), particle velocity (d) at the time of 415ps (G = 66 MW/cm^2).

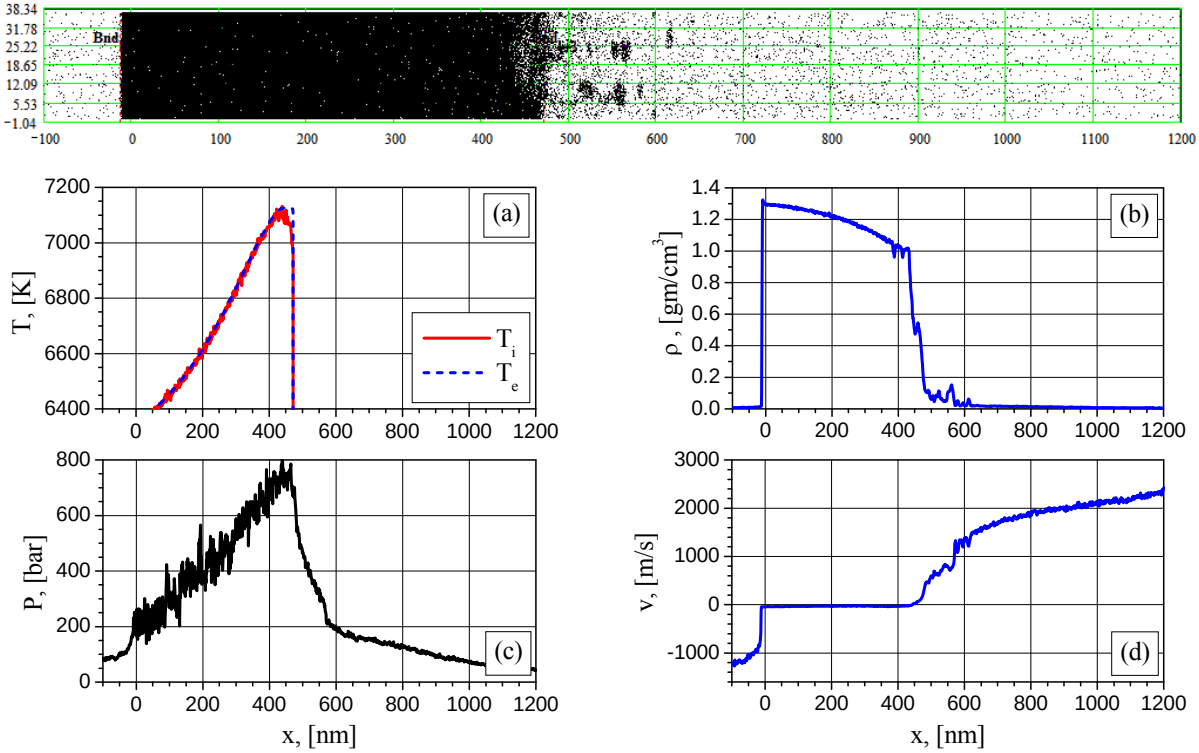

Fig. 11. 2D density particle distribution (snapshot) and 1D distributions of electron (blue) and ion (red) temperature (a), density (b), pressure (c), particle velocity (d) at the time of 595ps (G = 66 MW/cm^2).

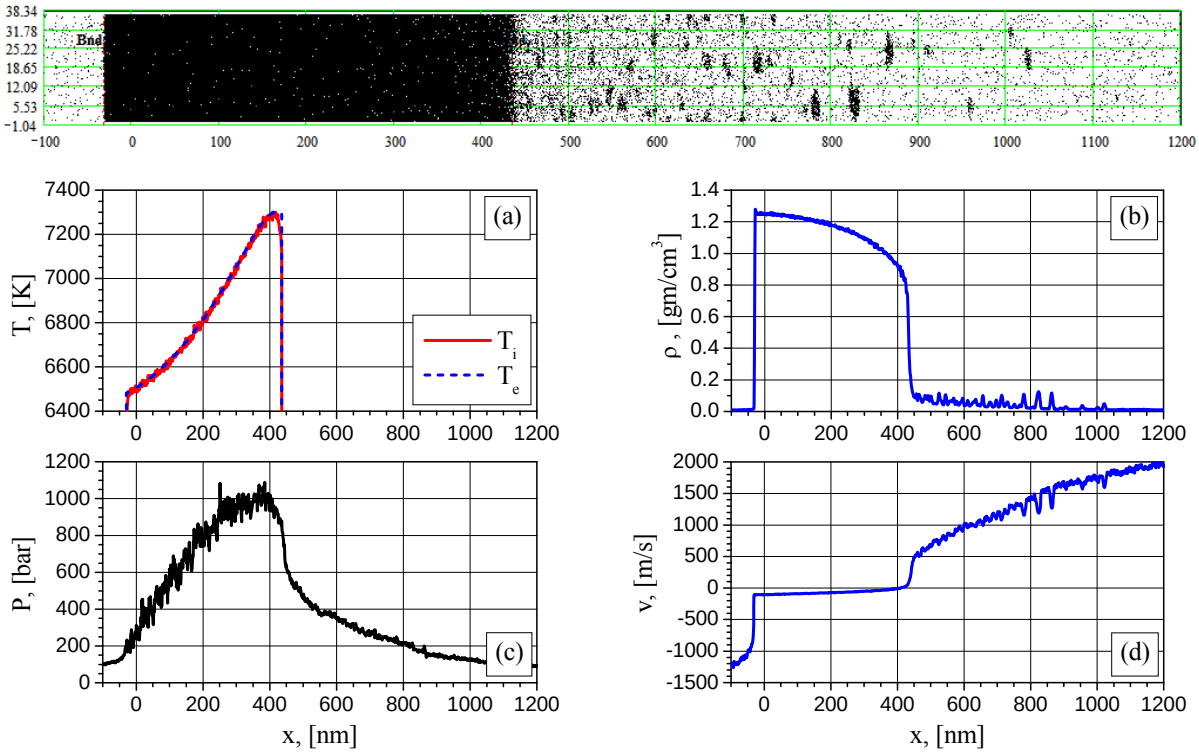

Fig. 12. 2D density particle distribution (snapshot) and 1D distributions of electron (blue) and ion (red) temperature (a), density (b), pressure (c), particle velocity (d) at the time of 900ps (G = 66 MW/cm^2).

REFERENCES

[1] A. Mazzi, A. Miotello. “Simulation of phase explosion in the nanosecond laser ablation of aluminum”, *Journal of Colloid and Interface Science* (2016), http://dx.doi.org/10.1016/j.jcis.2016.08.016

[2] A. Mazzi, F. Gorrini, A. Miotello. “Dynamics of liquid nanodroplet formation in nanosecond laser ablation of metals”, *Appl. Surf. Sci.* (2016), http://dx.doi.org/10.1016/j.apsusc.2016.09.006

[3] A. Mazzi, F. Gorrini, A. Miotello. “Liquid nanodroplet formation through phase explosion mechanism in laser-irradiated metal targets”, *Phys. Rev. E*, **92**, 031301 (2015).

[4] M.Q. Jiang, Y.P. Wei, G. Wilde, L.H. Dai. “Explosive boiling of a metallic glass superheated by nanosecond pulse laser ablation”, *Applied Physics Letters*, **106**, 021904 (2015).

[5] S. Celen. “On mechanism of explosive boiling in nanosecond regime”, *Appl. Phys. B*, **122**, 168 (2016).

[6] V.I. Mazhukin, A.V. Shapranov, M.M. Demin, A.A. Samokhin, A.E. Zubko. “Molecular dynamics modelling of nanosecond laser ablation: subcritical regime”, *Mathematica Montisnigri*, **37**, 24-42 (2016).

[7] A.A. Samokhin, S.I. Kudryashov, A.E. Zubko and A.V. Sidorin. “Modelling of nanosecond laser ablation. Continual approach”, *Mathematica Montisnigri*, **37**, 76-90 (2016).

[8] N.M. Bulgakova, A.V. Bulgakov. “Pulsed laser ablation of solids: transition from normal vaporization to phase explosion”, *Appl. Phys. A*, **73**, 199–208 (2001).

[9] S.I. Kudryashov, S. Paul, K. Lyon, S.D. Allen. “Dynamics of laser-induced surface phase explosion in silicon”, *Appl. Phys. Lett.*, **98**, 254102 (2011).

[10] V.I. Mazhukin, A.A. Samokhin, M.M. Demin, A.V. Shapranov. “Modeling of nanosecond laser vaporization and explosive boiling of metals”, *Mathematica Montisnigri*, **29**, 68-90 (2014).

[11] V.I. Mazhukin, A.A. Samokhin, M.M. Demin, A.V. Shapranov. “Explosive boiling of metals upon irradiation by a nanosecond laser pulse”, *Quantum Electronics*, **44**(4), 283-285 (2014).

[12] V.I. Mazhukin, A.A. Samokhin, A.V. Shapranov, M.M. Demin, P.A. Pivovarov. “On different regimes of condensed matter ablation depending on intensity and duration of absorbed electromagnetic pulses”, *PIERS Proceedings*, Prague, 2418-2421 (2015).

[13] V.I. Mazhukin, A.A. Samokhin, A.V. Shapranov, M.M. Demin. “Modeling of thin film explosive boiling—surface evaporation and electron thermal conductivity effect”, *Mater. Res. Express*, **2**, 016402 (2015).

[14] D.S. Ivanov and L.V. Zhigilei. “Combined atomistic-continuum modeling of short-pulse laser melting and disintegration of metal films”, *Phys. Rev. B*, **68**, 064114 (2003).

[15] V.I. Mazhukin. “Kinetics and Dynamics of Phase Transformations in Metals Under Action of Ultra-Short High-Power Laser Pulses. Chapter 8”, *In “Laser Pulses – Theory, Technology, and Applications”*, InTech., ed. by I. Peshko., 219-276 (2012).

[16] V.V. Zhakhovskii, N.A. Inogamov, Yu.V. Petrov, S.I. Ashitkov, K. Nishihara “Molecular dynamics simulation of femtosecond ablation and spallation with different interatomic potentials”, *Appl. Surf. Sci.*, **255**, 9592 (2009).

[17] A.A. Samokhin. “Some aspects of the intense evaporation of condensed media by laser radiation”, *Sov. J. Quantum Electron.*, **4**(9), 1144–1145 (1975).

Received December 20, 2016